Spatiotemporal Modeling for Image Time Series with Appearance Change: Application to Early Brain Development

James Fishbaugh[1], Martin Styner[2,3], Karen Grewen[3], John Gilmore[3], Guido Gerig[1]

[1] Department of Computer Science and Engineering, Tandon School of Engineering, NYU, NY
[2] Department of Computer Science, UNC Chapel Hill, NC
[3] Department of Psychiatry, UNC School of Medicine, NC

Abstract. There has been considerable research effort into image registration and regression, which address the problem of determining correspondence primarily through estimating models of structural change. There has been far less focus into methods which model both structural and intensity change. However, medical images often exhibit intensity changes over time. Of particular interest is MRI of the early developing brain, where such intensity change encodes rich information about development, such as rapidly increasing white matter intensity during the first years of life. In this paper, we develop a new spatiotemporal model which takes into account both structural and appearance changes jointly. This will not only lead to improved regression accuracy and data-matching in the presence of longitudinal intensity changes, but also facilitate the study of development by direct analysis of appearance change models. We propose to combine a diffeomorphic model of structural change with a Gompertz intensity model, which captures intensity trajectories with 3 intuitive parameters of asymptote, delay, and speed. We propose an optimization scheme which allows to control the balance between structural and intensity change via two data-matching terms. We show that Gompertz parameter maps show great promise to characterize regional patterns of development.

1 Introduction

Time series imaging data are commonly acquired in medical imaging studies. In the simplest form, changes are assessed between a baseline and follow-up scan. To facilitate comparison, image registration establishes voxel-wise correspondence so measurements can be directly compared between baseline and follow-up, or the registration deformation field can itself be studied as a description of change. When more than two scans are available, registration naturally gives way to regression, in order to model the inferred continuous image change. In either case, registration or regression, the problem is most often solved by a deformation of image structure; appearance changes are not explicitly modeled. Rather, differences in intensities between images are considered a hindrance to the estimation of accurate deformation fields. However, image intensity and local contrast may contain rich and valuable information. For example, the maturation process in the early developing brain manifests as rapidly increasing white matter intensity [1]. Recent work has demonstrated that MRI intensity and contrast measures

quantify patterns of early brain development, showing a brain maturation rate difference between males and females [2]. In this paper, we similarly seek to quantify early brain development by explicitly modeling intensity change over time as part of an image regression framework.

There has been tremendous research effort into accurate registration schemes in the presence of appearance changes. However, as previously mentioned, appearance changes are rarely handled explicitly. Rather, image similarity metrics such as mutual information or normalized cross correlation are used to reduce sensitivity to intensity differences. In the case of appearance change due to pathology, registration methods often involve masking, and thus require prior segmentation to aid in registration [3].

An approach to image matching which combines structural and intensity changes was proposed as image metamorphosis [4], and was later integrated into a geodesic regression framework [5], though the baseline image was assumed to be fixed to the earliest observations, and experimentation appeared limited to 2D. In the metamorphosis approach, image intensity change is smoothly interpolated for exact matching. However, intensity change under the metamorphosis model does not have a clear interpretation to answer clinical questions about development. Importantly, the study of intensity change trajectories *themselves* as a representation of development has not yet been explored.

For clear interpretation and straightforward statistical analysis, parametric models of image intensity have been proposed. This includes linear intensity models for registration [6] and atlas building [7], and a logistic image intensity model for longitudinal registration [8]. However, the method [8] requires a tissue segmentation which itself requires non-linear registration as a preprocessing step. The method of [9] proposes a parametric pharmacokinetic intensity model to improve accuracy in atlas building, for motion correction of dynamic contrast-enhanced MRI. Ultimately, these methods are registration schemes, which are inherently limited to estimating a discrete set of deformations, one for each image, rather than a single time-varying flow of deformation which more naturally captures longitudinal changes. Nevertheless, our work takes the spirit of these previous methods when it comes to modeling appearance, as we favor the parametric approach for the power to distill down complex patterns of development into a small number of easy to understand parameters.

To summarize, there has been considerable work in addressing appearance change for registration and atlas building, though there has been limited work on image regression with appearance change. Furthermore, the study of the intensity trajectories, either as curves or as parameters of functions, is a relatively unexplored topic. In other words, modeling image appearance change is not only a mechanism to achieve more accurate registration; intensity trajectories themselves contain rich information about development and warrant further study. In this paper, we propose a spatiotemporal model for image time series which explicitly models both structural and appearance change. Image deformations are modeled by diffeomorphic flow with a flexible and non-parametric acceleration based method [10]. We favor this image deformation model for its flexibility, however, one could instead choose from a variety of models, such as geodesic [11] or higher order models [12,13]. Intensity changes are modeled by a Gompertz function, which has three intuitive parameters of asymptote, delay, and speed. The deformation and intensity change models are motivated by the driving application of modeling brain

development from birth, which is characterized by early accelerated growth which saturates to an asymptote [14]. In contrast to previous work, our model requires no masking or prior segmentation, and simultaneously estimates *continuous* structural deformations along with parametric intensity change trajectories with a clear interpretation. Experimental validation on a synthetic image sequence as well as longitudinal MR images demonstrate that Gompertz parameter maps encode regional patterns of development using natural terms of speed and delay.

2 Methods

In this section, we describe the two main components of our proposed spatiotemporal model: the structural deformation model and the intensity change model. We then combine the two components and provide a least squares estimation procedure.

2.1 Structural Deformation Model

Here, we introduce the structural deformation model, first proposed in [15] for shape regression and more recently for image regression [10], with the main idea of parameterizing diffeomorphic flow by a time-varying function of acceleration. Acceleration is defined as

$$a(x,t) = \sum_{i=1}^{N_C} K^V(x, c_i(t))\alpha_i(t) \tag{1}$$

where an impulse vector field $\alpha_i(t)$ is attached to a sparse set of N_C control points $c_i(t)$ and smooth kernel operator K defining the reproducing kernel Hilbert space V (for example, a Gaussian with standard deviation σ_V^2). Given such a time-varying acceleration field, a flow of diffemorphisms of the ambient space can be computed by solving:

$$\ddot{\phi}(x(t),t) = a(x(t),t) \tag{2}$$

given initial position $x_0 = x(t_0)$ and initial velocity $v_0 = v(t_0)$. Solving Eq. 2 generates a flow of diffeomorphisms starting from identity $\phi(0) = Id$, which defines the trajectory of a point starting from $x(t_0)$ and ending at $x(T)$. Starting from a given distribution of control points $c_i(0)$, the continuous path of control points $c_i(t)$ is computed by solving Eq. 2. Just as with control points, coordinates of image voxels also evolve according to Eq. 2, starting from a baseline image $\boldsymbol{I}_0$. Therefore, given $\alpha_i(t)$, one can compute the continuous evolution of control points, and compute acceleration at physical image coordinates. This shows that the system can be parameterized by a finite number of parameters, given a time discretization of $\alpha_i(t)$.

From here on, let $\boldsymbol{\alpha}(t)$, $\boldsymbol{v}_0$, and $\boldsymbol{c}_0$ be the concatenation of the $\alpha_i(t)$'s, $v_i(0)$'s, and $c_i(0)$'s. Let a set of image observations in time range t_0 to T be written as $\boldsymbol{I}_{t_i} = (I_{t_1}, I_{t_2}, ...I_{t_n})$. The acceleration controlled deformation model can be leveraged for image regression by estimating impulse vectors $\boldsymbol{\alpha}(t)$, control point locations $\boldsymbol{c}_0$, and baseline image $\mathbf{I}_0$ which minimizes

$$E(\boldsymbol{\alpha}(t), \boldsymbol{c}_0, \boldsymbol{I}_0) = \sum_{i=1}^{N} d(\phi_{t_i} \circ \boldsymbol{I}_0, \boldsymbol{I}_{t_i})^2 + \gamma_A \int_{t_0}^{T} ||\mathbf{a}(t)||_V^2 dt \tag{3}$$

where d is a distance metric between images, γ_A weights the regularity of the time-varying acceleration $\mathbf{a}(t)$, and initial velocity $v_0 = 0$.

2.2 Gompertz Intensity Change Model

Motivated by the study of early brain development, we propose to model image appearance change with a Gompertz function. We believe the Gompertz function, which is a sigmoid curve, is a good fit for modeling early acceleration growth which eventually tapers off, which has been observed in MRI intensity of the developing brain [14]. The authors of [8] used similar reasoning to select a logistic appearance model, while the work of [16] found the Gompertz function to be an accurate model of diffusion measures during early development. The Gompertz function is written as: $g(t) = A\exp(-B\exp(-Ct))$ where $B > 0$ and $C > 0$.

One powerful feature of the Gompertz function is the straightforward interpretability of it's three parameters. The parameters A, B, and C, can be interpreted as asymptote, delay, and speed, respectively. This allows complex patterns of change to be communicated in simple terms that are naturally used to discuss development. We therefore propose the following Gompertz image appearance model:

$$\hat{I}(x,t) = g(x,t) = A(x)\exp(-B(x)\exp(-C(x)t)) \tag{4}$$

which describes continuous image appearance change over time t at location x. Gompertz parameters A, B, and C vary spatially, and can be thought of as parameter *images*. Later we will see how these parameter images can be analysed to study regional patterns of development. We will denote the appearance model at time t as $\hat{\mathbf{I}}(t)$.

2.3 Spatiotemporal Model With Appearance Change

We now propose a combined spatiotemporal model which simultaneously estimates continuous structural image deformations along with appearance change. The main difficulty in designing such a model is the inherent non-uniqueness in a solution which combines structural and appearance changes. As an example, consider an image of a

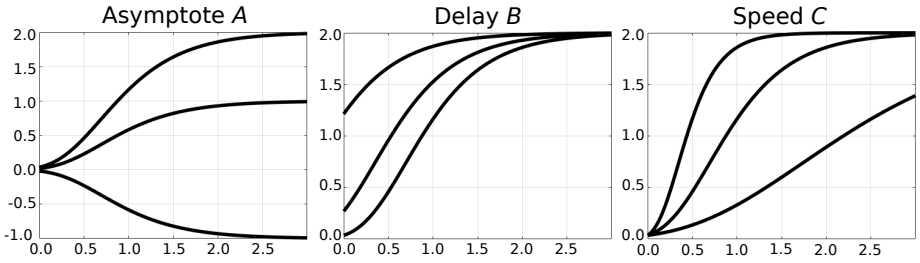

Fig. 1. The Gompertz function $g(t) = A\exp(-B\exp(-Ct))$ is parameterized by three intuitive values: asymptote, delay, and speed. In each plot, a range of values is plotted for each parameter while holding the other two fixed.

white circle which grows isotropically over time, but does not change appearance. The progression could be described completed by image deformations which capture the change in scale of the circle, or alternatively, entirely by an appearance model which "paints" in additional pixels. To address this issue, we allow for control over the contribution of the deformation and appearance models. This is accomplished with two data-matching terms, one measuring fit via deformation only, and one measuring fit by intensity change only. While this doesn't provide a globally optimal solution, it does allow the user to control estimation based on domain knowledge or empirical observation. Together with regularity terms, the model criterion is written

$$\begin{aligned} E(\boldsymbol{\alpha}(t), \boldsymbol{c}_0, A, B, C) = &\left[\sum_{i=1}^{N_{obs}} \lambda_D \; d(\phi_{t_i}(\hat{\mathbf{I}}(t_0)), I_{t_i})^2 + \lambda_A \; d(\hat{\mathbf{I}}(t_i), I_{t_i})^2 \right] \\ &+ \lambda_R \int_{t_0}^{T} ||\mathbf{a}(t)||_V^2 dt + \lambda_{TV} \; \mathrm{TV}(A, B, C) \end{aligned} \tag{5}$$

where the first two terms are data-matching by deformation only and intensity change only, the third term measures regularity of the time-varying deformation, and the last term is a total variation regularizer on the Gompertz parameters. We use an anisotropic version of total variation, which is differentiable. This term may be used promote regional consistency in asymptote, delay, and speed images, based on the assumption that tissue development is highly spatially correlated. For measuring image similarity d, we use sum-of-squared intensity difference. Weights λ allow to control the importance of each term in the overall cost. The final image sequence is then computed as $\phi_t(\hat{\mathbf{I}}(t))$.

Alternatively, the model may be expressed with a single data term measuring fit between observations and the generative model as $d(\phi_t(\hat{\mathbf{I}}(t)), I_{t_i})^2$. In this case, the relative contribution of the deformation and intensity model would be controlled entirely by regularity terms and weights λ_R and λ_{TV}. While this model is not explored in this paper, research into this and other formulations remains ongoing work with the goal of developing a robust and intuitive model of structural and appearance change.

Model estimation consists in finding time varying impulse vectors $\boldsymbol{\alpha}(t)$, location of control points $\boldsymbol{c}_0$, and Gompertz appearance parameters A, B, and C which minimize (5). The algorithm is initialized with $\boldsymbol{\alpha}(t) = \mathbf{0}$ (corresponding to no deformation), control points $\boldsymbol{c}_0$ on a regular grid with user selected spacing, and Gompertz appearance parameters $A = B = C = \mathbf{0}$. We implement a gradient descent scheme with gradients computed using autograd in PyTorch [17]. We also use KeOps (`http://www.kernel-operations.io`), which provides memory efficiency on the GPU, enabling the use of 3D image volumes on a TITAN Xp. Our implementation is available at `https://github.com/jamesfishbaugh/acceleration-diffeos`.

3 Experimental Validation

3.1 Synthetic Bull's-eye

We first validate our model on a synthetic image time series of a bull's-eye with both structural and appearance changes. The top row of Fig. 2 shows the observations of

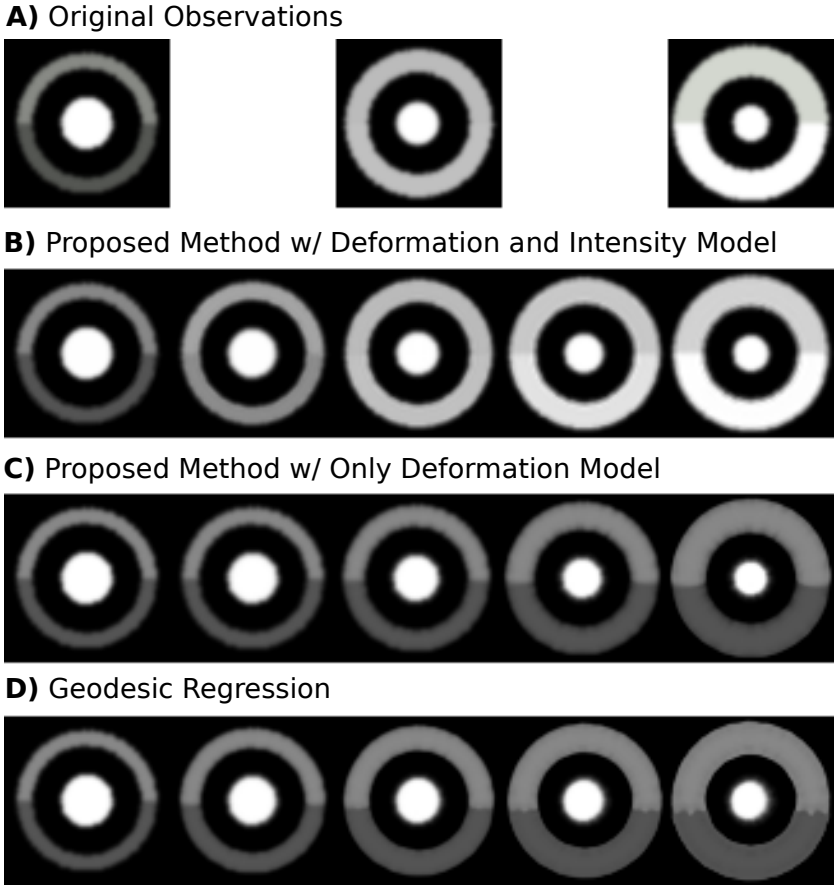

Fig. 2. Top) Synthetic observations representing the progression of a bull's-eye undergoing both structural and appearance changes. The outer ring grows while the inner circle shrinks. The bottom half of the outer ring shows a delay with respect to the top half, along with a faster increase in intensity. The inner circle does not change in appearance. **B) C) D)** Several frames from estimated continuous image trajectories under different models. Animation of our proposed method available at `https://youtu.be/5OqmLZOjalw`.

the bull's-eye images. The image sequence undergoes complex structural change, with the outer ring increasing in size over time according to an exponential, while the inner circle shrinks linearly. The outer ring is further characterized by two distinct patterns of appearance change. First, the bottom half shows a delay with respect to the top half. Second, intensity in the bottom half increases faster than intensity in the top region. The trajectory of change in the top half is given by a logistic function, while intensity in the bottom half changes linearly. The inner circle does not undergo any appearance change.

Fig. 2 B) shows the model estimated with our proposed method. Here we show only several frames, though the model can alternatively be viewed as a continuous animation

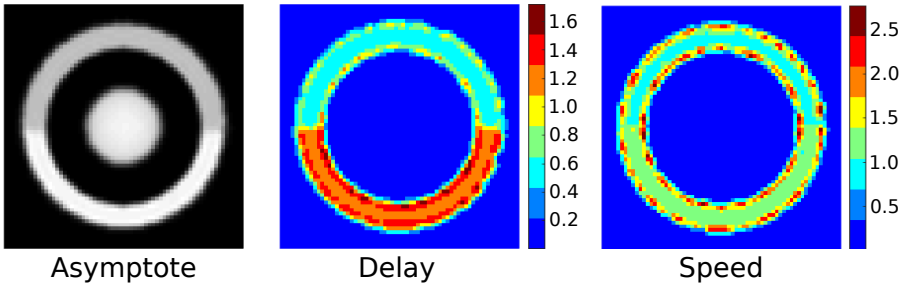

Fig. 3. Gompertz parameter images of asymptote A, delay B, and speed C for the synthetic bull's-eye progression from Fig. 2. The asymptote image most closely resembles the final image observation, representing intensity saturation. The lower half of the outer ring shows a significant delay with respect to the top half, as well as faster increase in intensity. The inner circle is not present in the delay and speed images, since the inner circle only undergoes structural changes.

for more intuitive understanding. The estimated image sequence very closely matches the observations, effectively capturing complex patterns of structural and appearance changes simultaneously. The average structural similarity was 0.99 while the average mean square error was 1.5×10^{-4}. Furthermore, our method provides realistic trajectories *between* observation time points, with smooth and continuous trajectories of both structure and appearance. For longitudinal data, this is a more natural representation of image change compared to a discrete set of diffeomorphisms, one for each image, which must be cascaded as in longitudinal registration [8].

We also estimated an image trajectory with a deformation model only, shown in Fig. 2 C). Here, we measured average structural similarity of 0.81 and average mean square error of 0.05. Finally, we compare against a readily available baseline method, a geodesic model using the software package Deformetrica [18], shown in Fig. 2 C), with an average structural similarity of 0.83 and average mean square error of 0.04.

We can explore a statistical representation of the appearance changes by investigating the Gompertz parameter maps, which are themselves images of the same dimension as the observations, shown in Fig. 3. The delayed and accelerated intensity region in the lower half of the outer ring is well captured by the delay and speed image, while the asymptote has similar characteristics to the final image observation.

3.2 Early Brain Development From Birth

Next, we seek to model structural and appearance change of the developing brain starting from birth. This is particularly challenging due to the rapid development and appearance changes observed in MR images during the first year of life. Imaging data consists of a longitudinal sequence of a healthy child scanned at birth, 1, 2, 4, and 6 years of age in the form of 3D T1W images of dimension 196x233x159 with 1x1x1 voxel size. Images were skull stripped and affine aligned. Intensity values across the entire longitudinal sequence were normalized to be between 0 and 1 based on min and max values across the longitudinal sequence. This is a naive normalization procedure

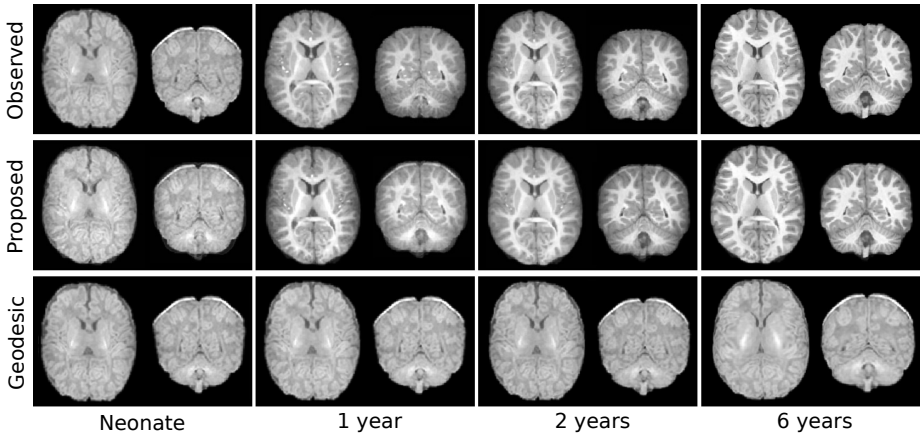

Fig. 4. Top) Observed T1W image sequence at birth, 1, 2, and 6 years of age. **Middle)** Images estimated by the proposed spatiotemporal model of structural and appearance change. Continuous evolution is better understood when viewed as an animation here: `https://youtu.be/AWsai9_dkhU`. **Bottom)** Image sequence estimated by a baseline geodesic model with no appearance model, which results in a unrealistic sequence which always maintains the appearance of a neonate.

that doesn't take into account scanner differences or possible hyperintense areas such as blood vessels. Although this procedure is suitable for proof of concept of our spatiotemporal model, proper normalization will have to be addressed in future work, to deal with the impact of non-calibrated scans acquired at different sites and even different scanner generations. However, longitudinal normalization of MR images comes with many challenges which are beyond the scope of this work.

To explore the impact of missing data, a model was estimated by excluding the year 4 observation. Fig. 4 shows the original observations (top) and the estimated image sequence from our proposed model (middle). Qualitatively, the model closely matches the observed image sequence, well capturing the observed image progression. Fig. 5 shows

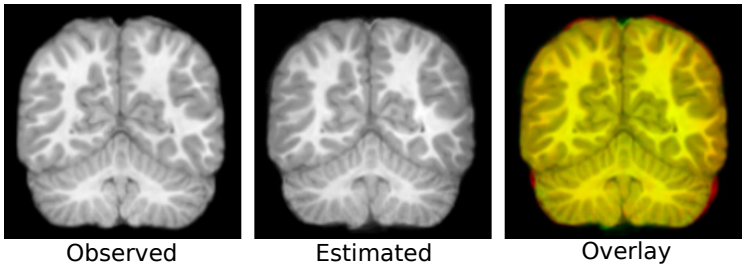

Fig. 5. Coronal slice from the 4 year old observation that was left out during model estimation, along with the image estimated by our model. The observed and estimated image are overlaid, with yellow indicating similar intensities, while red and green indicate intensity mismatch.

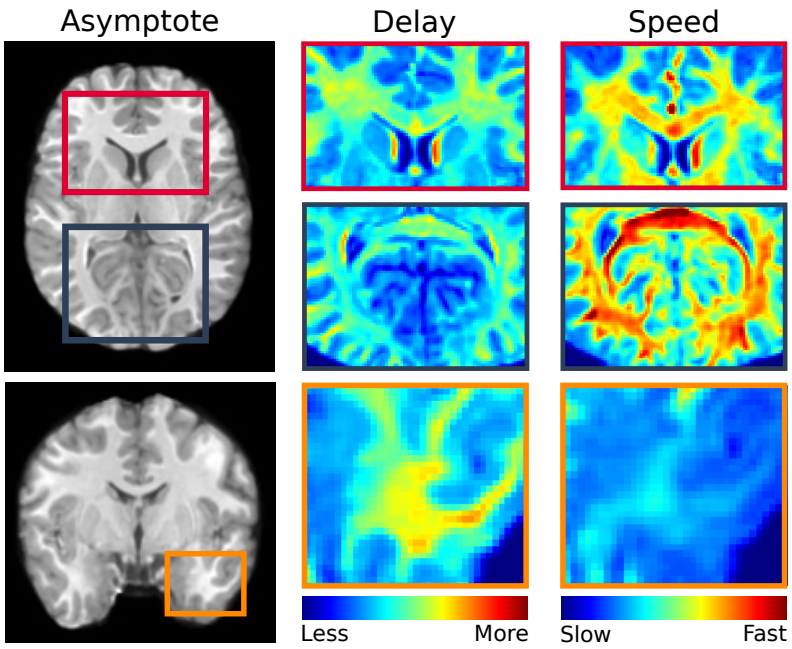

Fig. 6. Top) Gompertz delay and speed images capture a posterior to anterior pattern of growth, with the posterior region developing earlier and faster. **Bottom)** White matter development in the temporal lobe is delayed and progresses slowly compared to other regions.

that the smooth and continuous trajectory estimated by our method generates realistic images between observations, as the estimated image at 4 years old closely resembles the true 4 year old observation, which was not included in model estimation. We measured a structural similarity index of 0.93 and a root-mean-square error of 0.004. We also note the added benefit of a reduction in skull stripping artifacts in the estimated image compared to the original observation. The bottom row of Fig. 4 shows an unrealistic trajectory estimated with a geodesic model without considering appearance changes. It is worth noting that the geodesic model may also be estimated backward in time starting from 6 years old, or alternatively, estimated in both directions starting in the middle. However, all such models appear artificial and unrealistic since they all carry the appearance of their starting image.

Gompertz parameter images are shown in Fig. 6, which capture regional patterns of development. There is a clear posterior to anterior pattern of development captured in the delay and speed images. The anterior region shows increased delay and lower speed, while the posterior region is characterized by less delay and high speed. The temporal lobe also develops later, with relatively slow speed. These are all findings previously reported in pediatric radiology [1]. This can also been seen in Fig. 7 for selected regions of anterior white matter, posterior white matter, and also grey matter. It shows a pattern of delayed and slower white matter development in the anterior compared to the

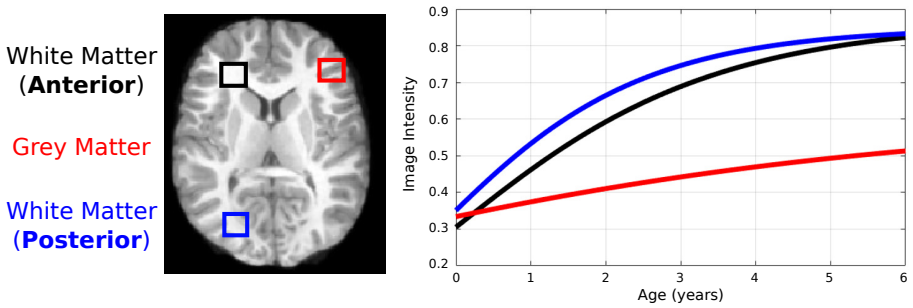

Fig. 7. Left) Selected regions of white and grey matter overlaid on estimated scan at 6 years old. Colored boxes are shown enlarged for illustration purposes, true regions are slightly smaller homogeneous 3D regions. **Right)** Regional averages of Gompertz parameters are shown from 0 to 6 years. We observe posterior white matter shows less delay than anterior white matter, but also undergoes accelerated development, reaching a shared asymptote quicker. Grey matter shows a more gradual linear increase in intensity over time.

posterior, which starts at a higher value and also reaches the asymptote more quickly. Grey matter, on the other hand, undergoes a slow, nearly linear, increase in intensity.

4 Discussion

Brain maturation can be observed as a change of intensity and contrast over time in MR images. In this paper, we proposed a spatiotemporal model which explicitly accounts for intensity change through a Gompertz appearance model. Our method estimates continuous structural and appearance change jointly, for a comprehensive description of early brain development. To overcome the problem of solutions being non-unique, we introduced two data-matching terms to balance the contribution of structural and appearance change. The problem could also be approached with an alternative cost function formulation, which is currently being explored as ongoing work. Another solution would be to limit appearance changes to white matter regions via a segmentation mask, as in [8]. In addition to estimating a continuous image sequence that closely matches observations, we showed that Gompertz parameter images capture patterns of development in intuitive terms of asymptote, delay, and speed. Since MRI intensity values are uncalibrated, the most pressing future work is longitudinal as well as population wide normalization, as in [19]. Longitudinal imaging studies face the challenge of acquisitions from different technicians from a variety of physical locations, as well as changes in scanner technology over the lifetime of a study, which make direct comparison of MRI intensities an open challenge. Directly comparing intensity across sites and scanner generation requires careful harmonization and normalization procedures.

Acknowledgments This work was supported by NIH grants NIBIB R01EB021391 (SlicerSALT), 1R01HD088125-01A1 (Down's Syndrome), 2R01HD055741-11 (ACE-IBIS), 1R01DA038215-01A1 (Cocaine Effects) and the New York Center for Advanced

Technology in Telecommunications (CATT). HPC resources used for this research provided by grant NSF MRI-1229185.

References

1. Rutherford, M.A., Bydder, G.M.: MRI of the Neonatal Brain. WB Saunders (2002)
2. Vardhan, A., Fishbaugh, J., Vachet, C., Gerig, G.: Longitudinal modeling of multi-modal image contrast reveals patterns of early brain growth. In: MICCAI. (2017) 75–83
3. Niethammer, M., Hart, G.L., Pace, D.F., Vespa, P.M., Irimia, A., Van Horn, J.D., Aylward, S.R.: Geometric metamorphosis. In: MICCAI. (2011) 639–646
4. Miller, M.I., Younes, L.: Group actions, homeomorphisms, and matching: A general framework. International Journal of Computer Vision **41**(1-2) (2001) 61–84
5. Hong, Y., Joshi, S., Sanchez, M., Styner, M., Niethammer, M.: Metamorphic geodesic regression. In: MICCAI, Springer (2012) 197–205
6. Periaswamy, S., Farid, H.: Elastic registration in the presence of intensity variations. IEEE Transactions on Medical Imaging **22**(7) (2003) 865–874
7. Gao, Y., Zhang, M., Grewen, K., Fletcher, P.T., Gerig, G.: Image registration and segmentation in longitudinal mri using temporal appearance modeling. In: IEEE ISBI. (2016) 629–632
8. Csapo, I., Davis, B., Shi, Y., Sanchez, M., Styner, M., Niethammer, M.: Longitudinal image registration with temporally-dependent image similarity measure. IEEE Transactions on Medical Imaging **32**(10) (2013) 1939–1951
9. Bhushan, M., Schnabel, J.A., Risser, L., Heinrich, M.P., Brady, J.M., Jenkinson, M.: Motion correction and parameter estimation in dcemri sequences: application to colorectal cancer. In: MICCAI. (2011) 476–483
10. Fishbaugh, J., Gerig, G.: Acceleration controlled diffeomorphisms for nonparametric image regression. In: IEEE ISBI. (2019) 1488–1491
11. Niethammer, M., Huang, Y., Vialard, F.X.: Geodesic regression for image time-series. In: MICCAI. (2011) 655–662
12. Singh, N., Vialard, F.X., Niethammer, M.: Splines for diffeomorphisms. Medical Image Analysis **25**(1) (2015) 56–71
13. Hinkle, J., Fletcher, P.T., Joshi, S.: Intrinsic polynomials for regression on riemannian manifolds. Journal of Mathematical Imaging and Vision **50**(1-2) (2014) 32–52
14. Dobbing, J., Sands, J.: Quantitative growth and development of human brain. Archives of Disease in Childhood **48**(10) (1973) 757–767
15. Fishbaugh, J., Durrleman, S., Gerig, G.: Estimation of smooth growth trajectories with controlled acceleration from time series shape data. In: MICCAI. (2011) 401–408
16. Sadeghi, N., Prastawa, M., Fletcher, P.T., Wolff, J., Gilmore, J.H., Gerig, G.: Regional characterization of longitudinal dt-mri to study white matter maturation of the early developing brain. Neuroimage **68** (2013) 236–247
17. Paszke, A., Gross, S., Chintala, S., Chanan, G., Yang, E., DeVito, Z., Lin, Z., Desmaison, A., Antiga, L., Lerer, A.: Automatic differentiation in pytorch. (2017)
18. Bône, A., Louis, M., Martin, B., Durrleman, S.: Deformetrica 4: An open-source software for statistical shape analysis. In: Shape in Medical Imaging. (2018) 3–13
19. Sweeney, E., Shinohara, R., Shea, C., Reich, D., Crainiceanu, C.M.: Automatic lesion incidence estimation and detection in multiple sclerosis using multisequence longitudinal mri. American Journal of Neuroradiology **34**(1) (2013) 68–73